The Astrophysical Journal Letters, 852:L19 (6pp), 2018 January 1 https://doi.org/10.3847/2041-8213/aaa28c
© 2018. The American Astronomical Society. All rights reserved.

Black Hole Formation and Fallback during the Supernova Explosion of a 40 $M_\odot$ Star

Conrad Chan[1,2], Bernhard Müller[1,3], Alexander Heger[1,4,5], Rüdiger Pakmor[2], and Volker Springel[2,6,7]
[1] Monash Centre for Astrophysics, School of Physics and Astronomy, Monash University, VIC 3800, Australia; conrad.chan@monash.edu
[2] Heidelberger Institut für Theoretische Studien, Schloss-Wolfsbrunnenweg 35, D-69118 Heidelberg, Germany
[3] Astrophysics Research Centre, School of Mathematics and Physics, Queen's University Belfast, Belfast BT7 1NN, UK
[4] School of Physics & Astronomy, University of Minnesota, Minneapolis, MN 55455, USA
[5] Center for Nuclear Astrophysics, Department of Physics and Astronomy, Shanghai Jiao-Tong University, Shanghai 200240, People's Republic of China
[6] Zentrum für Astronomie der Universität Heidelberg, Astronomisches Recheninstitut, Mönchhofstr. 12-14, D-69120 Heidelberg, Germany
[7] Max-Planck-Institut für Astrophysik, Karl-Schwarzschild-Str. 1, D-85740 Garching bei München, Germany
Received 2017 October 2; revised 2017 December 11; accepted 2017 December 12; published 2018 January 4

Abstract

Fallback in core-collapse supernovae is considered a major ingredient for explaining abundance anomalies in metal-poor stars and the natal kicks and spins of black holes (BHs). We present a first 3D simulation of BH formation and fallback in an "aborted" neutrino-driven explosion of a 40 solar mass zero-metallicity progenitor from collapse to shock breakout. We follow the phase up to BH formation using the relativistic CoCoNuT-FMT code. For the subsequent evolution to shock breakout we apply the moving-mesh code Arepo to core-collapse supernovae for the first time. Our simulation shows that despite early BH formation, neutrino-heated bubbles can survive for tens of seconds before being accreted, leaving them sufficient time to transfer part of their energy to sustain the shock wave as is propagates through the envelope. Although the initial net energy (∼2 Bethe) of the neutrino-heated ejecta barely equals the binding energy of the envelope, 11 $M_\odot$ of hydrogen are still expelled with an energy of 0.23 Bethe. We find no significant mixing and only a modest BH kick and spin, but speculate that stronger effects could occur for slightly more energetic explosions or progenitors with less tightly bound envelopes.

Key words: methods: numerical – stars: black holes – stars: massive – supernovae: general

1. Introduction

Often the collapse of massive stars results in the formation of a black hole (BH) instead of a neutron star. Observations of supernova progenitors suggest that a large fraction of stars above 15 $M_\odot$ … 18 $M_\odot$ collapse quietly to BHs (Smartt 2015), and first direct evidence for the disappearance of red giants is currently being discussed (Adams et al. 2017).

It appears, however, that BH formation does not always proceed quietly without any mass ejection. Even if no neutrino-driven or magnetohydrodynamically driven engine explodes the star, the loss of gravitational mass due to neutrino emission may lead to the (partial) ejection of the hydrogen envelope, giving rise to a faint red transient (Nadezhin 1980; Lovegrove & Woosley 2013).

BH formation may also occur in a full-blown supernova explosion. In the collapsar model (MacFadyen & Woosley 1999) for gamma-ray bursts and hypernovae, the formation of a BH with an accretion disk is central to the mechanism itself. In neutrino-driven explosions or magnetorotational explosions involving rapidly spinning neutron stars, BH formation can occur due to *fallback*, which pushes the neutron star above its maximum mass limit. Fallback can be "prompt" (Wong et al. 2014) when accretion onto the neutron star remains strong in the first seconds of an explosion, or occur at late times times when the reverse shock decelerates outgoing shells below the escape velocity (Chevalier 1989). Particularly strong fallback is expected for low explosion energies comparable to the binding energy of the stellar envelope (Zhang et al. 2008).

There is a body of evidence for fallback in supernova explosions. Transients with unusually low explosion energies and nickel masses have been interpreted as due to fallback (Zampieri et al. 2003; Moriya et al. 2010). Further evidence comes from extremely metal-poor (EMP) stars that were presumably polluted by the ejecta of one or at most a few supernovae from Population III (Pop III) progenitors. Abundance anomalies in such EMP stars like high [C/Fe] and [O/Fe] ratios have been interpreted as resulting from the removal of most of the iron-group ejecta from the polluting supernova by fallback but allowing for mixing from some inner shells into the ejecta (mixing-fallback model; Nomoto et al. 2006). The star J031300.36-670839.3 is the most famous example. To date, no iron at all was detected, only a very low upper limit for iron could be determined. It is thought to originate from a fallback supernova from a 60 $M_\odot$ (Keller et al. 2014) or 40 $M_\odot$ (Bessell et al. 2015) star. Even more direct evidence for BH formation associated with a supernova comes from the pollution of companions in some X-ray binaries (Israelian et al. 1999).

If there is a BH formation channel via fallback, then this also has implications for the BH mass and spin distributions, which are now becoming accessible through GW detections (Abbott et al. 2016) in addition to measurements of BH properties within the Milky Way (masses: Özel et al. 2010; spins: Liu et al. 2008; Miller & Miller 2014). It has also been suggested that asymmetric fallback can give rise to large BH kicks (Janka 2013), which would have repercussions on the evolution of binary systems with fallback supernova progenitors.

Understanding BH formation, fallback, and mixing in core-collapse supernovae calls for detailed numerical simulations. Late fallback due to outflow deceleration by the reverse shock can be studied (Zhang et al. 2008; Ertl et al. 2016) in spherical symmetry (1D), but multi-dimensional (multi-D) models are required to address mixing and the effect of the fallback on BH kicks and spins. Mixing and prompt fallback are intimately

connected to the asymmetries imprinted on the explosion by the neutrino-driven or MHD-driven supernova engine.

Although multi-D simulations of fallback and mixing due to the Rayleigh–Taylor instability—typically with a focus on massive Pop III progenitors—were conducted in 2D (Joggerst et al. 2009; Chen et al. 2017) and 3D (Joggerst et al. 2010a, 2010b), these were based on artificial 1D explosion models for the first seconds of the supernova. They thus miss the large-scale seed asymmetries that are provided by the supernova engine and that have been shown to decisively influence mixing out to late times in simulations starting from more consistent multi-D neutrino-driven explosions models of SN 1987A (Wongwathanarat et al. 2015) and Cas A (Wongwathanarat et al. 2017). They must also make ad hoc assumptions about the energetics of the explosion to achieve the desired fallback.

Here, we perform the first 3D simulations of a fallback supernova from the collapse stage through the onset of a neutrino-driven explosion, further through BH formation, and continued until shock breakout. Motivated by the abundance fits of Bessell et al. (2015) for the polluter of J031300.36-670839.3, we consider a $40M_\odot$ Pop III progenitor, although we do not attempt to reproduce any particular abundance pattern in this Letter. We rather seek to develop a basic understanding of explosions with strong fallback in multi-D: How is the energy transferred from the engine to the envelope? Are the $\sim 10^{51}$ erg from a neutrino-driven engine sufficient to unbind even part of an envelope with a much higher binding energy? If so, can efficient mixing develop during the explosion? What kick and spin is imparted onto the BH by asymmetric fallback?

2. Numerical Methods

2.1. Collapse to Black Hole Formation

We model the collapse of a non-rotating metal-free $40\,M_\odot$ progenitor evolved with the stellar evolution code *Kepler* (Heger & Woosley 2010). At the onset of core collapse, the model is mapped into the relativistic neutrino hydrodynamics code CoCoNuT-FMT (Müller & Janka 2015). The model has been simulated on a spherical polar grid with a resolution of $N_\mathrm{r} \times N_\theta \times N_\varphi = 550 \times 128 \times 256$ zones out to a radius of 10^5 km using a mesh coarsening scheme near the polar axis.

At high densities, we employ the nuclear equation of state (EoS) of Lattimer & Swesty (1991) with a bulk incompressibility modulus of $K = 220$ MeV, which allows for a maximum baryonic neutron star mass of $2.44\,M_\odot$. To precipitate shock revival, we artificially increase the strangeness contribution to the axial vector coupling for neutral current neutrino–nucleon scattering to an (unphysically large) value of $g_\mathrm{A,s} = -0.2$ as in Melson et al. (2015). This is justified as long as we merely seek to provide plausible initial conditions for the simulation of fallback and mixing after BH formation *assuming* that a neutrino-driven explosion occurs.

2.2. Black Hole Formation to Shock Breakout

After BH formation, we follow the evolution of the explosion until shock breakout using the quasi-Lagrangian moving-mesh hydrodynamics code Arepo (Springel 2010). Arepo solves the fluid equations in a finite-volume approach on an unstructured Voronoi mesh using adaptive time-stepping, second-order spatial reconstruction, and the HLLC Riemann solver. The position of the grid cells track the flow, providing resolution where it is needed in order to follow any mixing that develops in the frame of the rapidly expanding shock. The unstructured mesh of Arepo has no preferred directions, eliminating grid-alignment artifacts that sometimes plague traditional Eulerian hydrodynamics codes. We use the

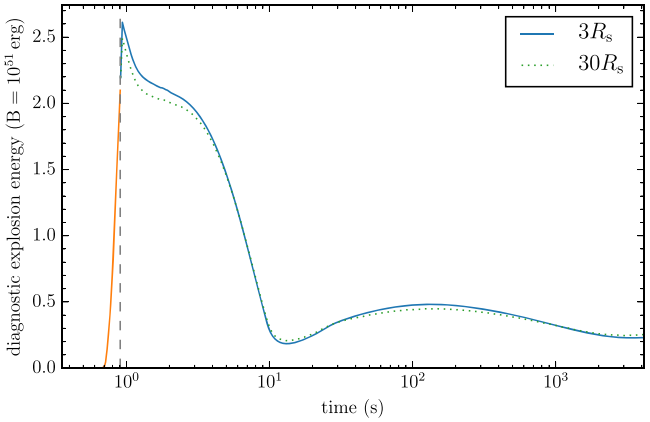

Figure 1. Diagnostic explosion energy during the CoCoNuT (orange) simulation and the Arepo (blue/green) simulations for different R_acc.

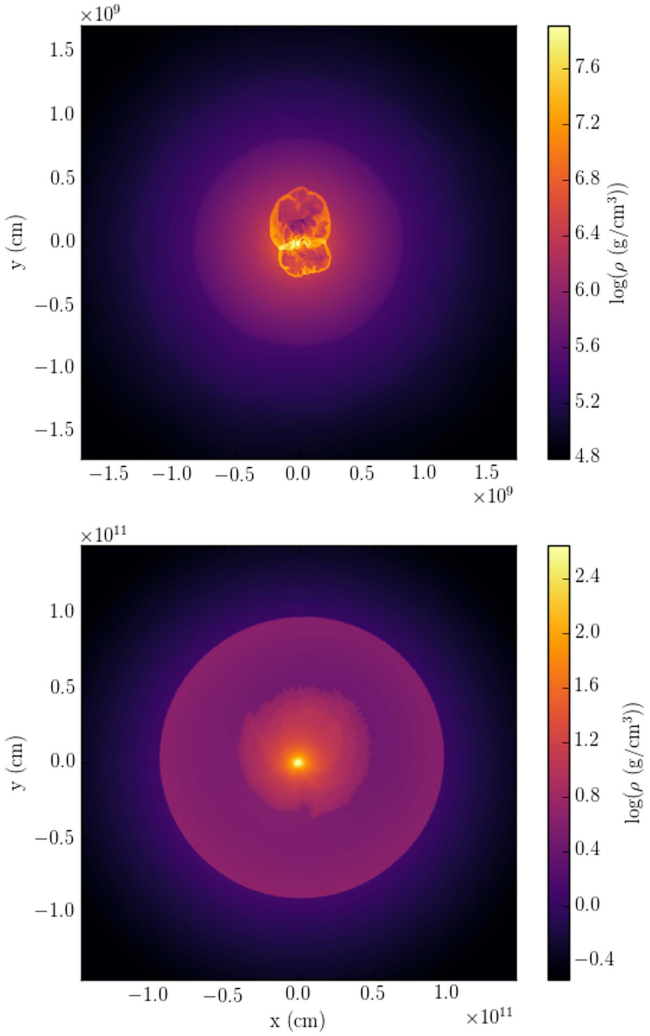

Figure 2. Top: density slice through the origin at BH formation (initial conditions for Arepo run). Bottom: density slice at 215 s, shortly after the explosion energy converges. At this stage, the shock is roughly spherically symmetric.

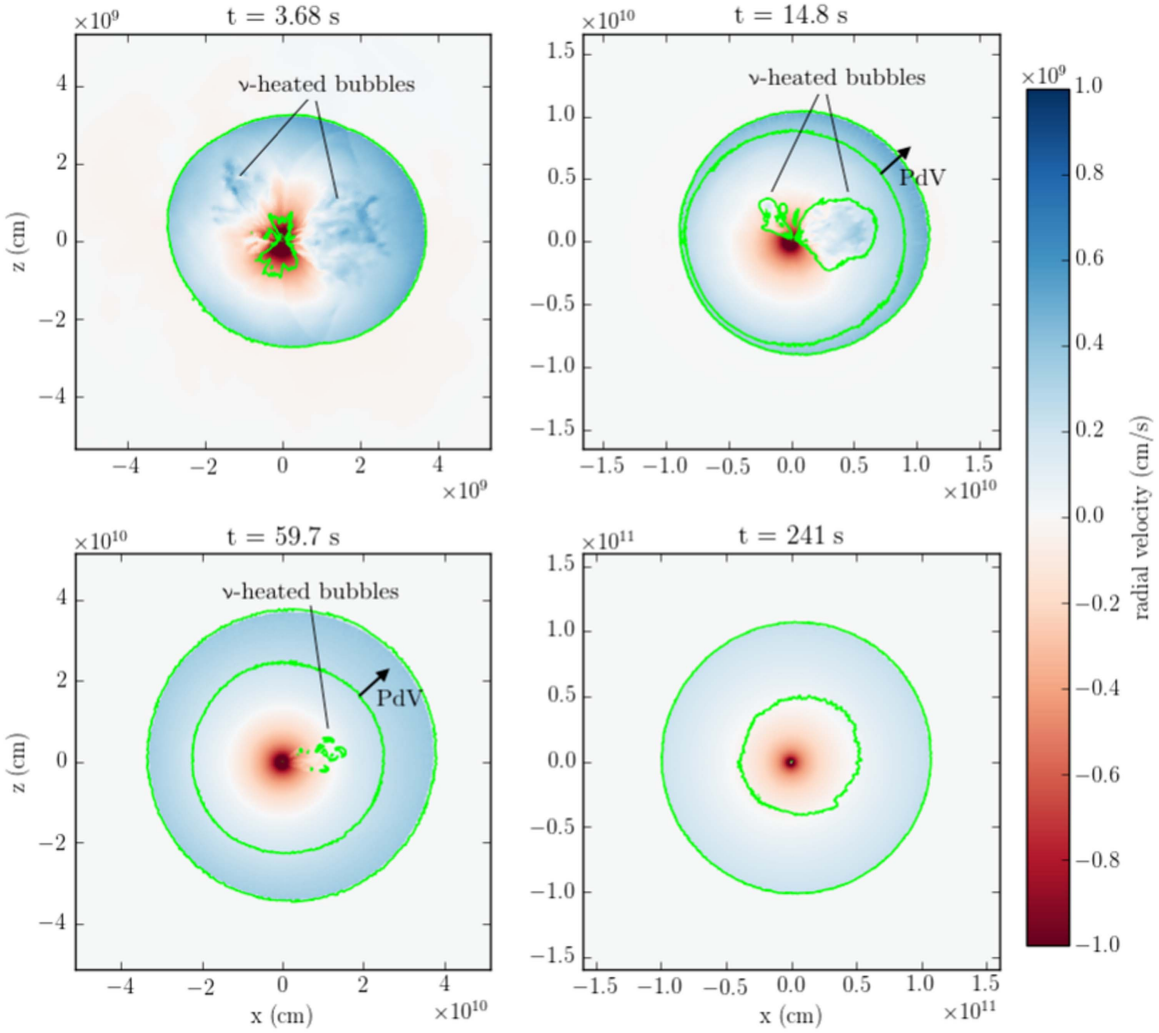

Figure 3. Radial velocity in a slice through the origin. Green isocontours indicate zero net energy. There exists a shell of material with negative diagnostic energy that is still expanding outward, depositing energy into the shocked material by $P\,dV$ work.

Helmholtz EoS (Timmes & Swesty 2000), which includes degeneracy and radiation pressure effects.

We account for the gravity of the BH by including the monopole potential of a point mass, and the self-gravity between gas cells is solved following Springel (2010) using a tree-based algorithm with a variable softening length with a spline function that varies from 10^3 to 10^8 km.

Except for the gravitational potential, periodic boundaries are used outside a box of 5×10^7 km width, which contains the entire star. An exponential isothermal atmosphere is adopted outside the star.

In order to map the CoCoNuT model into Arepo, we initialize a mesh-generating point at the geometric center of each grid cell. To achieve the target resolution, we apply cell refinement criteria based on the desired particle mass, such that the resolution is concentrated at regions of higher density. Since the CoCoNuT model only includes the region inside a radius of $R = 10^5$ km, we add the original 1D pre-supernova profile outside, which smoothly fits the 3D models since no significant changes have occurred at the fitting radius at the time of mapping. In the outer layers, we adopt a mesh-generating point configuration similar to Ohlmann et al. (2015), using nested shells of HEALPix configuration (Gorski et al. 2004). Due to small differences in the low-density EoS, we map the temperature instead of the internal energy density, which makes the mapping slightly non-conservative, but small conservation errors are unavoidable when mapping a GR model to a Newtonian code: we find a 0.3% change in total mass of 0.044 $M_\odot$ and 4.5% change in diagnostic explosion energy (Section 3) of 0.095 B.

To model the accretion onto the BH, we continuously remove all mass below a radius $R_{\rm acc} = 3\,R_{\rm s}$ (where $R_{\rm s}$ is the Schwarzschild radius of the BH) and add it to the central point mass.

3. Results

Due to the high progenitor mass, the model maintains high accretion rates after core bounce, and the proto-neutron star quickly grows in mass, reaching a baryonic mass of 2 $M_\odot$ in less than 0.2 s, and contracts rapidly. Such conditions are conducive (Müller et al. 2012) to violent activity of the standing accretion shock instability (SASI; Blondin et al. 2003). This helps stabilize the retraction of the average shock radius at about 100 km around 0.2 s after bounce. High electron flavor neutrino luminosities $\gtrsim 10^{53}$ erg s^{-1}, hard neutrino spectra, a small gain radius, and stabilization of the shock radius by the SASI result in high heating efficiencies and

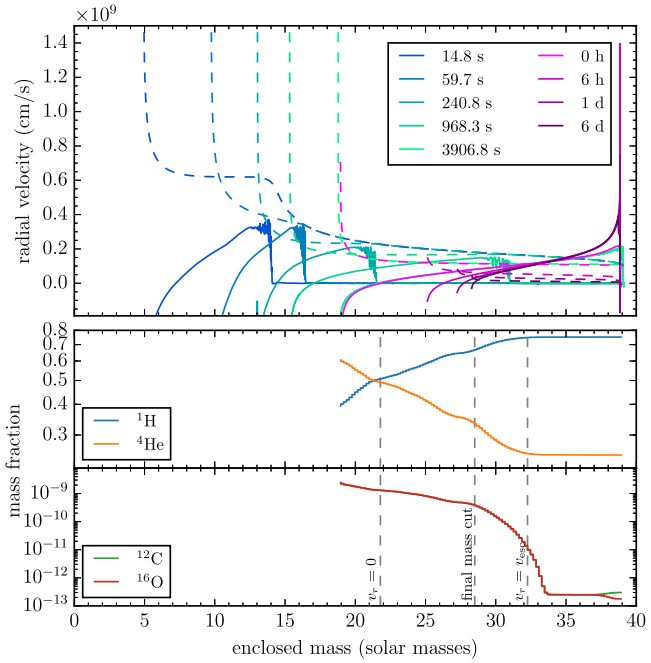

Figure 4. Top: radial velocity (solid lines) and escape velocity (dashed) as a function of enclosed mass at selected times up to shock breakout (blue/cyan) and after shock breakout (magenta/purple). Bottom: mass fractions as a function of mass coordinate at shock breakout. Dashed lines show the radii where $v_r = 0$ and $v_r = v_{esc}$ at breakout (left/right) and the final mass cut (middle).

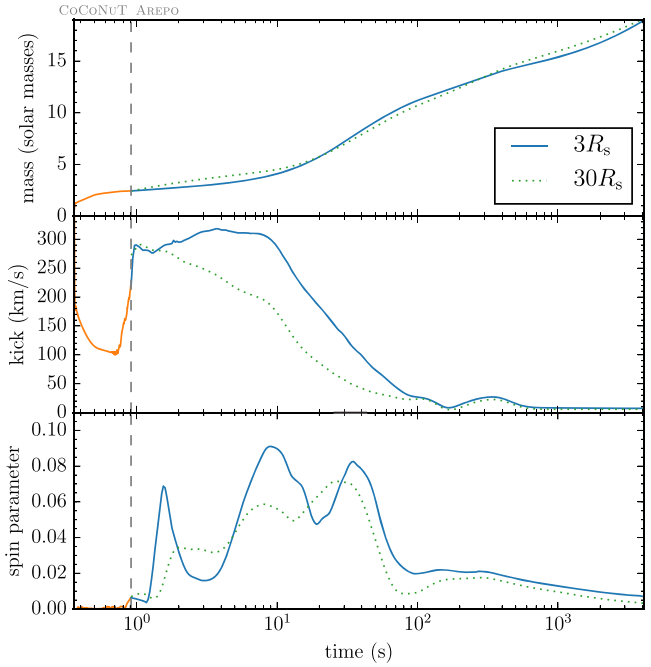

Figure 5. Top to bottom: mass, kick velocity v_{BH}, and spin parameter a of the central remnant for different R_{acc}.

eventually in shock revival 0.35 s after bounce. Due to our artificial reduction of the neutrino–nucleon scattering cross-section and due to the approximations in the FMT transport scheme, more rigorous simulations are needed to test whether this scenario for shock revival for rapidly accreting proto-neutron stars is indeed viable. It is, however, not implausible. The trend toward powerful SASI activity and high heating efficiencies for massive neutron stars is in line with other simulations, especially more systematic 2D studies (Burrows et al. 2016; Summa et al. 2016) that often obtain explosions more readily for more massive progenitors. Even if our neutrino treatment overestimates the heating conditions, it is plausible that other physical ingredients could drive our model into a neutrino-driven runaway, such as rapid rotation (Summa et al. 2017), auxiliary magnetic field effects (Obergaulinger et al. 2014), or enhanced neutrino luminosities due to novel microphysics at high densities (Bollig et al. 2017).

The diagnostic explosion energy E_{diag} is evaluated as in Müller et al. (2017) in the CoCoNuT run, and in the subsequent Arepo run the Newtonian limit (Buras et al. 2006) is used:

$$E_{diag} = \int_{e_{tot}>0} \rho e_{tot}\, dV, \quad (1)$$

$$e_{tot} = \epsilon_{int} + \frac{v^2}{2} - \frac{Gm}{r}, \quad (2)$$

where ρ, ϵ_{int}, e_{tot}, v, and m are the density, internal energy density (excluding rest-mass contributions), total net energy density, velocity, and enclosed mass at radius r. Although E_{diag} grows rapidly (Figure 1), BH formation due to ongoing accretion ensues 0.55 s after bounce.

At this time, two large neutrino-heated bubbles that expand in roughly opposite directions have pushed the shock to about 4000 km (Figure 2), and E_{diag} has reached a value of 2.09×10^{51} erg. This barely equals the binding energy, $E_{bind} = 2.1 \times 10^{51}$ erg of the shells outside the shock. One might therefore expect that the incipient explosion is quenched after BH formation.

3.1. Explosion Dynamics after Black Hole Formation

The neutrino-heated bubbles continue to expand for a significant time after BH formation in the Arepo run (Figure 3). Buoyancy allows these underdense bubbles to expand against the drag of the infalling shells and to maintain a positive net energy out to a radius of several 10,000 km, although turbulent mixing and drag slowly drain the positive diagnostic energy of the bubbles during the first seconds of the explosion. The bubbles only fall back onto the BH after tens of seconds. This provides them with sufficient time to transfer considerable energy and momentum to the matter swept up by the shock, which develops outward velocity and positive net energy outside a radius of ~100,000 km. When the bubbles undergo fallback, the shock wave remains sufficiently energetic to propagate to the stellar surface with a final explosion energy of 2.3×10^{50} erg. The evolution of E_{diag} is not monotonic. After a minimum at ~10 s, it rises until 100 s after bounce. This behavior is explained by Figure 3: energy can be transferred to the front of the shock wave by $P\,dV$-work even from inner shells with negative net energy, as long as they still expand. The energy transfer from the initial neutrino-heated ejecta, which eventually undergo fallback, to the propagating shock wave is operating until late times when the neutrino-heated bubbles no longer have positive net energy.

After a few tens of seconds, the shock wave becomes spherical and, as shown by radial velocity profiles in Figure 4, decelerates as it sweeps through the outer shells of the progenitor. At shock breakout, the outermost 18.2 $M_\odot$ have been accelerated to positive velocity. To determine late-time

fallback, we spherically average the model, map it into the finite-volume code PROMETHEUS (Fryxell et al. 1991), and evolve it until 6 days after shock breakout using a moving grid of 1200 radial zones with outflow boundary conditions at the inner boundary. The final mass cut emerges at a mass coordinate of 28.5 $M_\odot$. This is close to the point where the radial velocity equals the Keplerian orbital velocity at shock breakout. No reverse shock ever forms in this explosion. Instead, a rarefaction wave forms as the inner ejecta are decelerated by gravity and undergo fallback.

With an ejecta mass of $\sim$11 $M_\odot$, the observable transient should appear similar to a low-energy explosion of a moderately massive progenitor except for the absence of a nickel-powered tail. Relatively low ejecta masses of sub-energetic nickel-poor SNe IIP (Spiro et al. 2014) may thus not necessarily be an argument against a fallback origin. Future work needs to determine whether the combinations of explosion energy, ejecta mass, and non-zero nickel mass observed in contemporary supernovae can be obtained in slightly more energetic models and with different progenitors. The nickel tail could, however, be mimicked by the accretion luminosity from *late* fallback, which will affect about 0.2 $M_\odot$ of bound material with positive velocity, enough to provide the equivalent luminosity to a few 10^{-3} $M_\odot$ of nickel.

There is no discernible mixing during the propagation of the shock through the envelope. The ejected material therefore contains mostly hydrogen and helium, possibly with a tiny admixture of CNO elements and Ca from Pop III star hydrogen burning (Keller et al. 2014). This admixture is too small to explain C, O, and Mg abundance patterns in C-enhanced metal-poor (CEMP) stars like J031300.36-670839.3 with this particular realization of a fallback supernova. Further simulations with more favorable initial energetics are required for ejection of substantial amounts of intermediate-mass elements.

To investigate the robustness of our results to our approximations, we conducted a test with a larger accretion radius of 30 R_s. Although this means excising the innermost 170 km immediately after BH formation, this model is similar to the baseline model as exemplified by the evolution of the diagnostic energy (Figure 2). That the energetics prove insensitive to such a severe change of initial conditions also suggests that switching to the Newtonian approximation at BH formation is unproblematic for a first qualitative study. For quantitative validation, one needs fully general relativistic 3D neutrino hydrodynamics simulations (Ott et al. 2017) and needs to extend these beyond BH formation.

3.2. Remnant Properties

Initial asymmetries in the explosion can contribute to the kick and spin of the BH. We calculate the BH kick from the ejecta momentum assuming momentum conservation (Scheck et al. 2006):

$$\boldsymbol{v}_{\rm BH} = \frac{1}{M_{\rm BH}} \int_{\rm ejecta} \rho \boldsymbol{v}\, dV, \tag{3}$$

where ρ and $\boldsymbol{v}$ are the density and velocity, and $M_{\rm BH}$ is the instantaneous mass of the BH. The angular momentum $\boldsymbol{J}$ of the BH is obtained by integrating the angular momentum flux onto the central remnant:

$$\frac{d\boldsymbol{J}}{dt} = 4\pi r_*^2 \int \rho(\boldsymbol{r} \times \boldsymbol{v}) d\Omega, \tag{4}$$

where r_* is a fiducial radius outside the accretion radius. For numerical evaluation this requires averaging the angular momentum flux in a thin shell around r_*. From this, one can determine the BH spin parameter, a:

$$a = \frac{cJ}{GM^2}. \tag{5}$$

Figure 5 shows a, BH mass, and kick velocity. The kick is already substantial ($\sim$200 km s^{-1}) at BH formation and continues to increase until 10 s. Asymmetric accretion transiently spins up the BH to $a = 0.09$. Once the asymmetric neutrino-heated ejecta have undergone fallback and the shock becomes spherical, however, the BH kick and spin converge to low values. At breakout we find $v_{\rm BH} \sim 10$ km s^{-1} and $a \sim 0.01$. The evolution of the kick and spin is more strongly affected by moving the accretion radius to 30 R_s in the comparison run than the diagnostic energy, though the final values are again similar. This is unsurprising and merely demonstrates the severity of the test, which involves cutting out the highly asymmetric flows inside a radius of 180 km right away.

Our model cannot explain the high natal BH kicks of several 100 km s^{-1} that have been inferred by some authors for individual BH low-mass X-ray binaries (Repetto et al. 2012, 2017; but see Mandel 2016 for a critical assessment). Our results suggest, however, that fallback could be a viable explanation for such large kicks if the kick were to freeze out close to the maximum values during the simulation. This could happen if large asymmetries survive until late times, either because of incomplete fallback in a more energetic explosion, or because part of the outer shells are removed, e.g., by binary interaction. By contrast, even if the spin were to freeze out near its maximum value, the spin-up of the BH by fallback would be insufficient to account for the unexplained high spin parameters in some high-mass X-ray binaries (Moreno Méndez 2011). This indirectly supports the theory that high spin parameters require special evolutionary channels for fast progenitor rotation (Moreno Méndez 2011).

4. Conclusions

We presented the first 3D simulations that follow BH formation and fallback in a core-collapse supernova from the collapse of the progenitor's iron core through shock revival by the neutrino-driven mechanism to BH formation using the neutrino hydrodynamics code CoCoNuT-FMT and then on to shock breakout using the moving-mesh code Arepo. Our simulations, conducted for a 40 $M_\odot$ Pop III star, indicate that neutrino-driven explosions that undergo BH formation due to sustained accretion after shock revival can still shed a large fraction of the stellar envelope even if the initial explosion energy is comparable to the binding energy of the envelope. In our case, an initial explosion energy of 2×10^{51} erg proves sufficient to eject 11 $M_\odot$ with a final explosion energy of 2.3×10^{50} erg. Despite using an approximate transport scheme and a reduced neutrino–nucleon scattering rate, our model suggests that the neutrino-driven engine can become rather powerful close to BH formation, energizing explosions with powers of $\sim 5 \times 10^{51}$ erg s^{-1} due to high accretion rates and heating efficiencies.

Our simulation of the explosion dynamics and the remnant properties after BH formation showed that neutrino-heated ejecta can evade fallback onto the BH for several seconds, giving them sufficient time to transfer part of their energy and

momentum to the outer layers behind the propagating shock wave. In our model, few traces of the initial asymmetries survive until late stages, however. There is complete fallback of the He core, and no products from the inner shells are mixed into the ejecta. The only change to the primordial composition of the progenitor is a tiny enrichment in C, N, O, and Ca from hydrogen burning in Pop III stars. This by itself would not be sufficient to explain abundances in CEMP stars like J031300.36-670839.3. Similarly, we do not yet find the large BH kicks that have been claimed by some authors (Repetto et al. 2012).

Our study constitutes a first step toward the exploration of BH formation and fallback based on 3D supernova explosion models. Open questions for future investigation include whether the neutrino-driven mechanism can indeed operate in massive stars of $\sim 40\,M_{\odot}$. This has to be explored using simulations with more rigorous neutrino transport and without artificial changes to the neutrino opacities. The parameter space for fallback to produce viable models for the polluters of some CEMP stars, nickel-poor transients, and BHs with high kicks and spins must be determined. Whether fallback supernovae can explain all of these phenomena in cases with an adequate ratio between the initial explosion energy and the binding energy of the envelope will be studied in future simulations.

This research was undertaken with the assistance of resources from the National Computational Infrastructure, which is supported by the Australian Government, and from the Pawsey Supercomputing Centre with funding from the Australian Government and the Government of Western Australia. We acknowledge support by ARC grants FT120100363 (A.H.) and FT120100363 (B.M.), STFC grant ST/P000312/1 (B.M.), by JINA-CEE through US NSF grant PHY-1430152, and by the European Research Council through ERC-StG grant EXAGAL-308037 (V.S./R.P.) and thank the Klaus Tschira Foundation (V.S./R.P.).

ORCID iDs

Alexander Heger https://orcid.org/0000-0002-3684-1325
Volker Springel https://orcid.org/0000-0001-5976-4599

References

Abbott, B. P., Abbott, R., Abbott, T. D., et al. 2016, PhRvX, 6, 041015
Adams, S. M., Kochanek, C. S., Gerke, J. R., Stanek, K. Z., & Dai, X. 2017, MNRAS, 468, 4968
Bessell, M. S., Collet, R., Keller, S. C., et al. 2015, ApJL, 806, L16
Blondin, J. M., Mezzacappa, A., & DeMarino, C. 2003, ApJ, 584, 971
Bollig, R., Janka, H.-T., Lohs, A., et al. 2017, PhRvL, 119, 242702
Buras, R., Janka, H.-T., Rampp, M., & Kifonidis, K. 2006, A&A, 457, 281
Burrows, A., Vartanyan, D., Dolence, J. C., Skinner, M. A., & Radice, D. 2016, SSRv, in press (arXiv:1611.05859)
Chen, K.-J., Heger, A., Whalen, D. J., et al. 2017, MNRAS, 467, 4731
Chevalier, R. A. 1989, ApJ, 346, 847
Ertl, T., Ugliano, M., Janka, H.-T., Marek, A., & Arcones, A. 2016, ApJ, 821, 69
Fryxell, B., Arnett, D., & Müller, E. 1991, ApJ, 367, 619
Gorski, K. M., Hivon, E., Banday, A. J., et al. 2004, ApJ, 622, 759
Heger, A., & Woosley, S. E. 2010, ApJ, 724, 54
Israelian, G., Rebolo, R., Basri, G., Casares, J., & Martín, E. L. 1999, Natur, 401, 142
Janka, H. T. 2013, MNRAS, 434, 1355
Joggerst, C. C., Almgren, A., Bell, J., et al. 2010a, ApJ, 709, 11
Joggerst, C. C., Almgren, A., & Woosley, S. E. 2010b, ApJ, 723, 353
Joggerst, C. C., Woosley, S. E., & Heger, A. 2009, ApJ, 693, 1780
Keller, S. C., Bessell, M. S., Frebel, A., et al. 2014, Natur, 506, 463
Lattimer, J. M., & Swesty, F. D. 1991, NuPhA, 535, 331
Liu, J., McClintock, J. E., Narayan, R., Davis, S. W., & Orosz, J. A. 2008, ApJL, 679, L37
Lovegrove, E., & Woosley, S. E. 2013, ApJ, 769, 109
MacFadyen, A. I., & Woosley, S. E. 1999, ApJ, 524, 262
Mandel, I. 2016, MNRAS, 456, 578
Melson, T., Janka, H.-T., Bollig, R., et al. 2015, ApJL, 808, L42
Miller, M. C., & Miller, J. M. 2014, PhR, 548, 1
Moreno Méndez, E. 2011, MNRAS, 413, 183
Moriya, T., Tominaga, N., Tanaka, M., et al. 2010, ApJ, 719, 1445
Müller, B., & Janka, H.-T. 2015, MNRAS, 448, 2141
Müller, B., Janka, H.-T., & Heger, A. 2012, ApJ, 761, 72
Müller, B., Melson, T., Heger, A., & Janka, H.-T. 2017, MNRAS, 472, 491
Nadezhin, D. K. 1980, Ap&SS, 69, 115
Nomoto, K., Tominaga, N., Umeda, H., Kobayashi, C., & Maeda, K. 2006, NuPhA, 777, 424
Obergaulinger, M., Janka, H.-T., & Aloy, M. A. 2014, MNRAS, 445, 3169
Ohlmann, S. T., Röpke, F. K., Pakmor, R., & Springel, V. 2015, ApJL, 816, L9
Ott, C. D., Roberts, L. F., da Silva Schneider, A., et al. 2017, arXiv:1712.01304
Özel, F., Psaltis, D., Narayan, R., & McClintock, J. E. 2010, ApJ, 725, 1918
Repetto, S., Davies, M. B., & Sigurdsson, S. 2012, MNRAS, 425, 2799
Repetto, S., Igoshev, A. P., & Nelemans, G. 2017, MNRAS, 467, 298
Scheck, L., Kifonidis, K., Janka, H.-T., & Müller, E. 2006, A&A, 457, 963
Smartt, S. J. 2015, PASA, 32, e016
Spiro, S., Pastorello, A., Pumo, M. L., et al. 2014, MNRAS, 439, 2873
Springel, V. 2010, MNRAS, 401, 791
Summa, A., Hanke, F., Janka, H.-T., et al. 2016, ApJ, 825, 6
Summa, A., Janka, H.-T., Melson, T., & Marek, A. 2017, ApJ, in press (arXiv:1708.04154)
Timmes, F. X., & Swesty, F. D. 2000, ApJS, 126, 501
Wong, T.-W., Fryer, C. L., Ellinger, C. I., Rockefeller, G., & Kalogera, V. 2014, arXiv:1401.3032
Wongwathanarat, A., Janka, H.-T., Müller, E., Pllumbi, E., & Wanajo, S. 2017, ApJ, 842, 13
Wongwathanarat, A., Müller, E., & Janka, H.-T. 2015, A&A, 577, A48
Zampieri, L., Pastorello, A., Turatto, M., et al. 2003, MNRAS, 338, 711
Zhang, W., Woosley, S. E., & Heger, A. 2008, ApJ, 679, 639